

**Mapping vegetation structure of arboreal wildlife habitat enclosures using
drone-derived Structure from Motion photogrammetry and spectral
vegetation indices**

Research Paper for the Marshall Plan Foundation

by

Brenna Yunn Fowler MSc

Department of Geography

San Diego State University

Supervisor Host Institution:

Dr. Gernot Paulus

Department of Geoinformation and Environmental Technologies

Carinthia University of Applied Science

Supervisor Home Institution:

Dr. Douglas Stow

Department of Geography

San Diego State University

Table of Contents

- Table of Figures 2
- List of Equations 3
- Abstract 4
- Acknowledgments..... 5
- Introduction..... 6
- Literature Review..... 7
 - Wildlife Monitoring & Habitat Suitability..... 7
 - Leveraging New Technology: Remote Sensing & GIS 7
 - Methodological Insights & Best Practices 8
 - Structure from Motion (SfM) Photogrammetry 9
 - Inverse Watershed Segmentation (IWS)..... 9
 - Spectral Vegetation Indices (SVI) 10
- Materials & Methods 10
 - Overview..... 10
 - Study Area 12
 - Image Acquisition..... 14
 - Image Processing 15
 - Deriving Vegetation Structure Metrics 16
 - Structure Classes and Gap Analysis..... 16
 - Individual Tree Identification and Delineation 17
 - Tree Species and Health Assessment..... 20
- Results..... 21
- Discussion 29
 - Implications for Wildlife Management..... 29
 - Challenges 30
 - Future Work 31
- References..... 33
- Appendix..... 37

Table of Figures

Figure 1: Methodological Workflow Diagram.....	11
Figure 2: Study Area: Affenberg Landskron.....	12
Figure 3: Ground Photos of Enclosure: a.) central area of enclosure; b.) outer periphery; c.) swamp-wetland areas; d.) shrubs and herbaceous understory; e.) wood structures and natural features	13
Figure 4: IWS Workflow.....	19
Figure 5: Canopy Measurement: a.) canopy polygons (teal) that are converted to lines (green); b.) simplified crown polygons (green lines) with centroids (teal dot); c.) CHM (rainbow) with polygon layer (black) and IWS tree points (black dots)	20
Figure 6: T1 & T2 Height Models (CHM) over respective orthomosaics (ortho)	22
Figure 7: Canopy Height Model (CHM) map of potential sleeping locations.....	23
Figure 8: Vegetation Structure Classification	24
Figure 9: Individual Trees (Digitized vs IWS).....	25
Figure 10: Tree species in structure classes: Evergreen & Deciduous.....	26
Figure 11: Canopy Gaps from T1 & T2 with the light green being the openness areas during leaf - off periods, the blue being leaf - on periods, and the darker green areas being year-round	27
Figure 12: CHM changes between T1 & T2	28
Figure 13: Tree Health Assessment using NDVI: Green areas represent high to moderate NDVI of 0.4 – 1.0, yellow areas with NDVI between 0.2 – 0.4, and red areas below 0.2.	29
Figure 14: NDVI frequency distribution.....	29

List of Equations

Equation 1: Canopy Gaps	17
Equation 2: Normalized Difference Vegetation Index (NDVI).....	20

Abstract

This study focuses on mapping vegetation structure within an arboreal wildlife habitat enclosure, Affenberg- Landskron in Villach, Austria, using drone imagery and Structure from Motion (SfM) photogrammetry, spectral vegetation indices (SVI), and GIS techniques. This project aims to enhance understanding of the spatial distribution of vegetation and its impact on habitat suitability for a population of Japanese macaque monkeys (*Macaca fuscata*). Through multiple drone flights capturing leaf – on and leaf – off conditions, high – resolution visible (RGB) imagery was collected and processed to create canopy height models (CHM), a Normalized Difference Vegetation Index (NDVI) images, and applicable thematic maps. The study used an image segmentation technique, Inverse Watershed Segmentation (IWS), to automate the delineation of individual tree crowns and diameters. CHM was used to generate the baseline datasets to classify vegetation structure and perform gap analysis, enabling a detailed assessment of canopy structure and openness. Health and species classification of either evergreen or deciduous trees was performed utilizing spectral indexing and thresholding. Seasonal differences in gaps and canopy cover revealed significant changes between temporal conditions which can influence macaque behavior and habitat use. The analysis highlights specific areas with vertical and horizontal vegetation complexity in providing suitable habitats for macaques, offering insights into optimal foraging and resting site availability. The findings underscore the value of remote sensing tools in ecological monitoring, providing repeatable and less labor-intensive methods to assess and monitor habitats in semi – natural enclosures. This study demonstrates the potential for integrating SfM photogrammetry, automated tree mapping, and SVI datasets to improve habitat monitoring for wildlife management applications.

Acknowledgments

I would like to take this opportunity to express my sincerest gratitude to Dr. Gernot Paulus for the research support and many resources you shared during my short but impactful stay in Villach, Austria. Thank you, Dr. Adrijana Car, for providing transportation as well as all the GIS assistance; your support made getting around and tackling this project much easier. Equally, my deepest thanks to my advisor and mentor, Dr. Douglas Stow, for providing continual direction and instruction, even with a 13-hour time difference.

Thank you to the Affenberg biologist Dr. Lena Pflüger for facilitating my memorable time with the macaque monkeys – a fun experience up close and personal. Thank you, Mr. Ulf Scherling, for your generous drone and computer operational support, and Dr. Stefan Ruess, for your outstanding remote sensing technical expertise.

Last but not least, I am grateful to the logistical support staff at Carinthia University of Applied Sciences (CUAS) Fachhochschule Kärnten and the Marshall Plan Scholarship Foundation for this opportunity to study abroad. Thank you to Ms. Claudia Kraif, Ms. Aleksandra Jama, and Ms. Stephanie Steiner for your guidance and the outings you organized with the other international students.

Danke Schön !

Introduction

Affenberg Landskron, being a research center for primatologists, simultaneously serves as a visitor and educational facility providing guided tours. It is home to approximately 170 Japanese macaque monkeys whose population, and dynamics have been under observation for the last 25 years [16]. This facility inherited the only population of Japanese macaques (*Macaca fuscata*) to be translocated to Austria with the intention of conducting scientific research into population dynamics, demographic data, and social behaviors. The Austrian Research Promotion Agency FFG's BRIDGE program has begun an interdisciplinary research project that investigates novel toolsets to enhance and compliment the traditional behavioral research methodology for monkey studies. The SIENA research group (Spatial Informatics for ENvironmental Applications) at the Carinthia University of Applied Sciences (CUAS) pioneers this technological advancement by implementing digital data collection, ranging from thermal- infrared object detection to "monkey facial recognition" machine learning modeling.

The significance of this specific Marshall Plan research project lies in habitat-level spatiotemporal pattern analysis of translocated Japanese macaque species. In these types of structured environments, park managers have prioritized the wildness of wildlife species, by not marking, tattooing, or chipping the monkeys to identify individuals. This leaves a knowledge gap into the social dynamics and behaviors of the monkeys, especially in the sense of habitat preferences, where observations are only capable in the daylight hours and sleeping arrangements remain a mystery. The ultimate goal for bridging this gap is to decrease the investment of time and resources population survey work requires, specifically to arboreal wildlife in protected enclosures. The objective of this project is to observe, automate and map vegetation structure and habitat characteristics utilizing UAS- SfM photogrammetry, GIS, and image segmentation techniques in a protected enclosure for macaque monkeys. It aims to answer these research questions:

1. How does the spatial distribution of tree species, vegetation heights, and structure vary within the wildlife enclosure?
2. What are the temporal differences in vegetation structure characteristics for leaf-on and leaf-off conditions?
3. What areas in the enclosure can have the strongest influence on habitat suitability?

Literature Review

Wildlife Monitoring & Habitat Suitability

Japanese macaques (*Macaca fuscata*) inhabit a diverse range of forested and mountainous environments, often marked by dense canopies and fluctuating climates that demand adaptability. Within these habitats, they live alongside many of their own kind, forming intricate social networks built on dynamic connections. These networks continuously evolve, influenced by individual decisions as well as environmental pressures that shape the population. Social groups may split and share the same territory, adapting or redefining relationships based on changing conditions. Understanding these shifting dynamics is essential for accurately interpreting species behavior, improving management practices in captivity, and effectively protecting wild populations. Yet, studying macaque social structures is challenging, requiring meticulous tracking of individual animals and consistent, long-term documentation of behaviors. This work demands highly skilled researchers dedicated to detailed and persistent observations to truly capture the complexities of these social systems. Traditional methods of research based wildlife observations and experimental studies are time consuming, and labor intensive, especially in documenting species with the intention of preserving their natural states [1,2].

Ecosystem structure variables and the occurrence of species are strongly linked, as emphasized in current ecology research. As so, the measurement and characterization of vegetation structure through remote sensing and image processing can serve as a covariate for predicting animal occupancy [3]. Vegetation structure can directly affect the number and distribution of animals by foliage height diversity, availability of food sources, and heterogeneity in structure [3,4]. Furthermore, the vertical and horizontal vegetation structure, density, and patchiness affect species diversity and occurrence [5]. Habitat selection is observed in behaviors like foraging, nest placement, migration, and breeding [4].

Leveraging New Technology: Remote Sensing & GIS

Recent advances in remote sensing have propelled investigations into employing the proper tools to support forest ecology and mapping research [6]. Previous studies have evaluated the efficiency and value that satellite imagery, uncrewed aerial systems (UAS), geospatial analysis, and machine learning classifiers provide for mapping and monitoring forest composition and structure [7–11]. A few innovative studies combining UAS and Structure from Motion (SfM)

photogrammetry and multispectral data demonstrate their synergy for estimating and mapping vegetation structural attributes [12–14]. In such studies, UAS datasets that were validated using field datasets were shown to be reliable for estimating forestry metrics such as canopy cover, canopy height, tree density, canopy base height, canopy bulk density, tree stress, and wildfire burn severity [15,16].

Methodological Insights & Best Practices

Wildlife survey methods have evolved in recent years with the transition into automated and non- traditional techniques, incorporating artificial intelligence (AI), machine learning (ML), and convolutional neural network (CNN). For instance, Lyu et al. (2024) leveraged object-detection and remote sensing technologies to conduct a wild animal census and monitoring in in-situ heterogeneous habitats. By developing an ML model based on Faster R- CNN, they demonstrated that customized anchor boxes and a fusion of multi-feature maps significantly improved the model's capability to detect wild deer in low- resolution thermal UAS imagery.

Similarly, innovative research collaborations have explored digital technology for monkey distribution detection, particularly within the Affenberg enclosure. Notable contributions include theses by Lukas et al. (2021) and Yang et. al. (2020), who trained a CNN model with YOLO v3 for monkey facial recognition using video sequences [17]. This promising work continues under the Smart Monkey Lab, led by SIENA researchers, as they refine and expand the model's capabilities.

Building on this progress, a particularly relevant study to our project is the 2022 research by Mirka et al., which elucidated the necessary environmental parameters and UAS protocol for thermal infrared detection of macaques [18]. This pushed forward a new set of tools that helped inform and standardize how to monitor this species, taking into consideration limited accessibility and monkey camouflage within tree canopies. Altogether, a fusion of RGB and TIR orthomosaics proved valuable for estimating group populations, as clusters of monkeys were detected, potentially indicating sleeping site locations. Key findings indicate that an optimal above ground level (AGL) altitude for UAS operations is 120 m, with a minimum staging distance of 100 m for launch. These parameters established a reliable and repeatable method for conducting arboreal animal presence- absence surveys in ex- situ forested areas. This effectively minimizes monkey

responses to anthropogenic noise, a pertinent example of innovative science adhering to animal welfare protocols.

Structure from Motion (SfM) Photogrammetry

Remote sensing is increasingly capable of observing ecologically relevant factors, including dynamics of terrestrial habitats, patterns of forest structure, vegetation species composition, and inter-zonal landscape changes. Innovations in photogrammetric techniques have assisted natural resource management and agricultural operations in economically collecting and manipulating data on terrestrial ecosystems [19,20]. In particular, Structure from Motion (SfM) photogrammetry is an approach that employs image-matching algorithms using highly overlapping 2D images to estimate and generate 3D models of a scene. It utilizes stereoscopic parallax to identify corresponding features or image match points, ultimately producing a cloud of points. These dense point clouds (x, y, z) can then produce useful elevation and topographical information, such as digital terrain models (DTM) and digital surface models (DSM). SfM photogrammetry has gained popularity for being an affordable alternative to airborne laser scanning, such as light detection and ranging (LiDAR)[8]. SfM has been utilized for mapping crop production [21], monitoring fine- scale forest habitat changes [22], and supporting forest inventories[23]. Canopy and gap cover, vegetation height, and plant density can be estimated with dense point cloud data generated from UAS imagery [24–26].

Inverse Watershed Segmentation (IWS)

While identifying individual trees is relatively straightforward for the human eye, it remains a complex process for image-processing algorithms [27]. Stand density, or identifying the number of trees, can be a challenging endeavor in thick and occluded forests. One innovative technique to enhance delineation in complex areas is Inverse Watershed Segmentation (IWS), a GIS method that employs image segmentation to delineate objects in dense or complex areas of interest [28]. This intuitive process is useful for individual tree crown delineation (ITCD) using inverted canopy height models (CHM). In this dataset, the highest features (assuming built features are omitted) such as tree tops become low points or “basins” and the lowest points such as gaps between trees become the high points or “ridges.” This simulates the flow of water which can be useful for watershed algorithms that segment lower areas. These treetops or “basins” resemble where water would accumulate in a topographic depression. The boundaries are delineated around the basins which resemble the tree crowns. The final product of this segmentation routine can

identify individual trees through recognizing seed points or marker-control region-growing segmentation. These seeds serve as “hints” to the small regions or predefined points in the image that guide the segmentation process. There are different criteria to delineate these regions such as color, texture or geographic data which, for using CHM rasters, is height.

Spectral Vegetation Indices (SVI)

The use of spectral vegetation indices (SVI) for quantifying and mapping structural properties of vegetation has gained widespread acceptance. Prošek & Šímová (2019) explored enhancements in detailed vegetation mapping by integrating spectral information with 3D point clouds, showcasing improved capability to measure vegetation structural complexity [29]. Ustin & Gamon (2010) demonstrated that canopy reflectance can be closely linked to the three dimensional structure of vegetation stands [30]. Building on this premise, Taddeo et al. (2019) found a strong correlation between SVI metrics and the physical attributes of wetland ecosystems, including leaf area, orientation, density, and the proportion of plant material [31]. SVIs derived from field reflectance spectroscopy [32], UAS- RGB orthomosaics [33], or multispectral imagery [34], have been utilized alongside SfM vegetation canopy data.

Classification of vegetative species can be dependent on many image capture variables, such as understory reflectance, shadowing, and luminosity –even during the same flight acquisition. Fawcett et. al (2020) explored the utility of drones for precise monitoring of phenology across individual tree crowns, tracking the specific seasonal stages for floristic species [35]. Spectral variation is of prime interest for species discrimination especially in determining optimal single date time windows [36]. Lisein et. al (2015) found that spectral separability is of special concern when using orthophoto mosaics and that, specifically, an autumnal time window in temperate European forests can be optimal for deciduous species classification [36]. Furthermore, Adamczyk and Osberger (2014) conducted a separability analysis to identify effective SVIs for threshold-based classification of disturbances in Austrian forests, finding specific red- edge indices that demonstrated the most spectral separability to monitor forest health [37].

Materials & Methods

Overview

This section provides an overview of the methods used in this research project. It begins with a description and map of the study site, accompanied by on- the- ground images, followed by

the details for image acquisition using UAS and the processing of imagery into SfM raster datasets. Subsequently, it delves into the methodology for deriving vegetation structure metrics and their application in analyzing the wildlife enclosure. This includes a detailed explanation of the GIS approach for identifying vegetation structure classes, both temporally and spatially, using IWS and SVIs. A comprehensive methodology workflow is also presented in Figure 1 to outline each step of the process and ensure clarity in the analysis.

During this research project, three aerial flights and one ground-based survey were conducted to collect true color and multispectral imagery and ground reference points: One “leaf - off” or T1 dataset: 04/04/2024; Two “leaf - on” or T2 datasets: a.) 07/17/2024, b.) 09/17/2024; Ground reference points: 07/12/2024. Of those three flights, two were used for the temporal changes observed for leaf - off and leaf - on conditions (T1a and T2a), and the third captured multispectral imagery used for vegetation indices (T2b). Ground images seen in Figure 3 were taken during the GNSS collection.

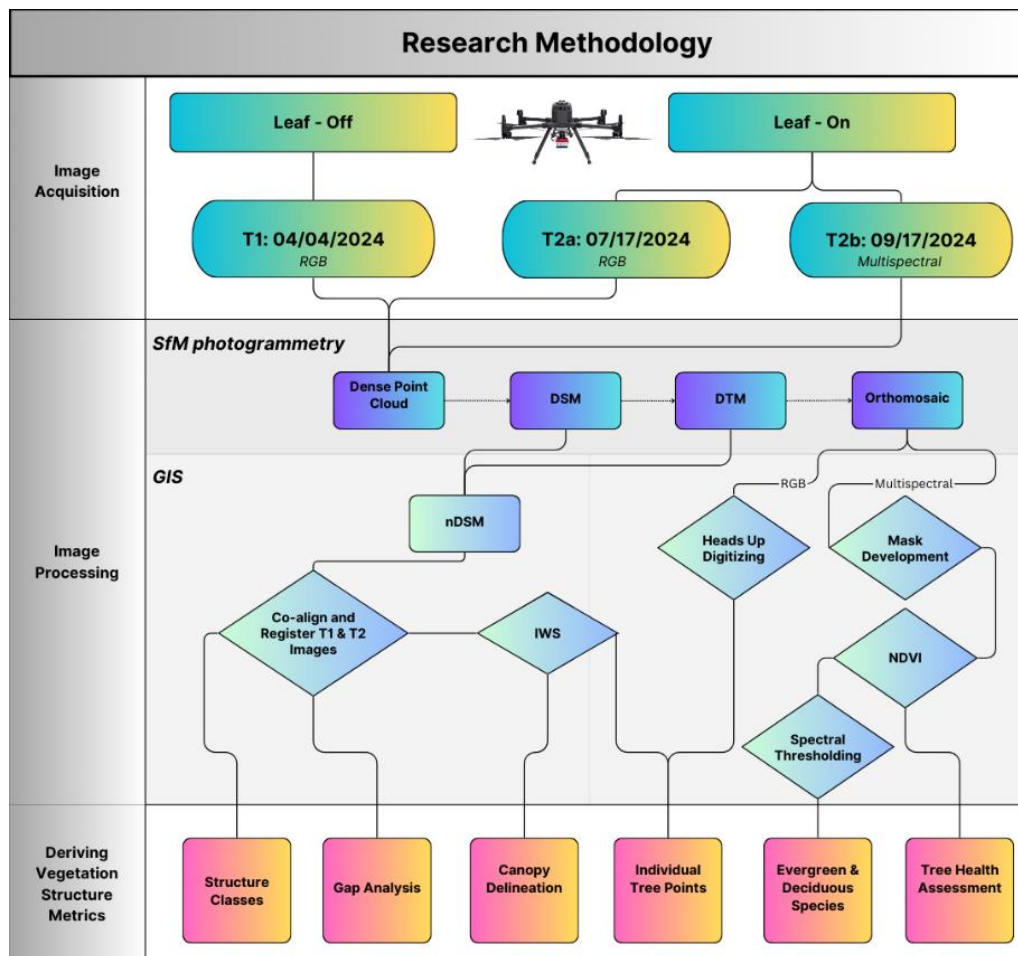


Figure 1: Methodological Workflow Diagram

Study Area

Our study area, seen in Figure 2, focuses on a 42,000 m² outdoor wildlife enclosure, Affenberg Landskron (translated to “Monkey Mountain”), which is located in Villach, Carinthia, in southwestern Austria. This part of Central Europe has a climate with four distinct seasons of hot and humid summers to snowing and below freezing winters [38]. Its habitat encompasses the natural mixed forest seen in Southern Austria which includes evergreen species such as Norway spruce (*Picea abies*), Scots pine or European red pine (*Pinus sylvestris*), deciduous species such as willow (*Salix* spp.), and various shrubs and herbs such as elderberry (*Sambucus nigra*), common hazel (*Corylus avellana*), raspberry (*Rubus idaeus*), nettle (*Urtica* spp), butterbur (*Petasites* spp), wood sorrel (*Oxalis* spp), and mixed grasses (*Poaceae*) [38].

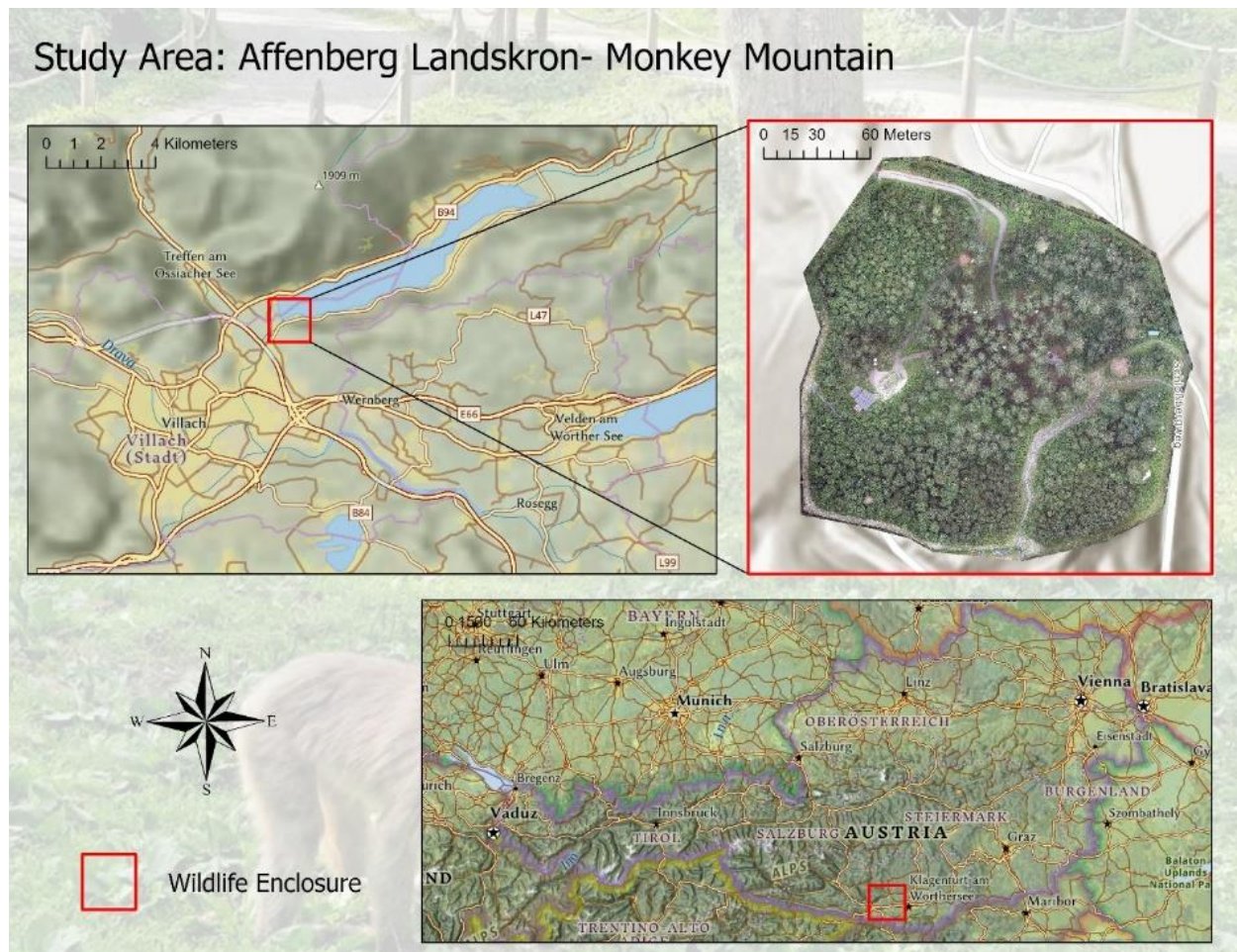


Figure 2: Study Area: Affenberg Landskron

The macaques are free-roaming and mostly congregate in the center of the enclosure where the forest floor is sparse, food is provided, and most of the group interact. Staff are able to monitor the group during daylight hours such as feeding times twice a day and through walking field

surveys throughout the central and peripheral areas. The natural vegetation in the enclosure provides grazing and foraging opportunities for the macaques alongside water sources for drinking. Some of the main physical features are: a small streambed, wetland area, a wooden hut building, a cement pool, and two free-standing shipping containers that are on the farther reaches from the central area. Experimental cooperation devices (games) that administer food are located in the center, where biologists perform noninvasive studies on the macaque's cognitive capabilities. There are many paved 2 m wide walking paths throughout and a protective 3.3 m high electric fence to keep macaques inside and native predators out. This outer peripheral fencing has densely vegetated slopes and then a buffer zone of 6 m of grassland and gravel. Visual examples of free-roaming macaques and their environment are provided in Figure 3.



Figure 3: Ground Photos of Enclosure: a.) central area of enclosure; b.) outer periphery; c.) swamp-wetland areas; d.) shrubs and herbaceous understory; e.) wood structures and natural features

Image Acquisition

UAS imaging was conducted using automated flight missions with pre- set parameters of platform height, distance, and speed. The sensor and platform used for this project are equipped with dual visible (RGB) and an 11- band multispectral instrument: a Zenmuse P1 RGB and Micasense RedEdge- MX DUAL imaging system mounted on a Matrice 350 RTK UAS. The spatial resolution of the UAS image collection is very fine, with a ground sampling distance (GSD) of 2.48 cm for RGB and 6.38 cm for multispectral. All flights were conducted with camera orientation nadir pointing with a minimum 80% sequential image forward and sideward overlap, ideal for stereoscopic parallax. This high amount of overlap is essential for SfM processing, by enabling a high number of match points to be identified from a range of geometric perspectives. Match points are used in the stereo-correlation and bundle block adjustment processing that enables 3D point cloud and orthomosaic generation. A Leica survey grade GNSS receiver was used to collect ground control points (GCP) for georeferencing T1 and T2 rasters. Due to the receiver signal strength, collecting GCPs was limited to only the areas of the enclosure not obscured by heavy canopy cover. These measurements were distributed near or on top of fixed developed features with sharp edges, such as the swimming pool and field hospital in the western section of the enclosure. Band specifics for the Micasense system can be seen in Table 1: Micasense Dual band specifics.

Table 1: Micasense Dual band specifics

Input Bands:
B1 - Blue-444
B2 - Blue
B3 - Green-531
B4 - Green
B5 - Red-650
B6 - Red
B7 - Red edge-705
B8 - Red edge
B9 - Red edge-740
B10 - NIR

The geometric processing of the UAS image data involved orthorectification to rectify distortions arising from the Earth's curvature and rotation effects. The projected coordinate system used for the entire project is Militar-Geographische Institut (MGI) Austria GK Central (EPSG

31255) and is based on the MGI geographic coordinate system (EPSG 4312) in Transverse Mercator (meters).

Image Processing

We used SfM photogrammetry in Agisoft Metashape (version 2.0) to produce dense 3D point clouds from the overlapping RGB images captured by the UAS. Four raster products per mission were generated from the 3D point clouds: a digital surface model (DSM), a digital terrain model (DTM), a normalized digital surface model (nDSM), and an orthoimage mosaic. The dense point cloud data represents the volumetric structure of the scene. The DSM depicts surface elevation in gaps between vegetation and the highest points of features, such as the tops of vegetation canopies. The DTM represents ground surface elevations. The nDSM depicts the difference between the DSM and the DTM, representing canopy heights.

A comprehensive workflow was implemented to generate the primary datasets for the study. This includes applying a statistical outlier filter for refining 3D coordinates and employing three gradual selection models to optimize image match points [22]. The first is a reconstruction uncertainty model that selects points that have a low statistical value of being accurately placed in the dense point cloud and then deleted. The second is a reprojection error model that gathers and deletes approximately 10% of the inaccurately matched points. The last model estimates projection accuracy, which finds more inaccurately projected points and deletes them. Manual inspection for outlier points was conducted, collectively contributing to the final optimization of camera alignment, orientation, and distortion reduction [39]. These steps are essential for the subsequent generation of dense point clouds for each mission.

Utilizing Agisoft Metashape's algorithm, points within dense point clouds were classified as either ground or nonground using an unsupervised classifier. After the classification step, a manual review of the ground points was performed through an iterative adjustment of classification results by visual assessment of respective orthomosaics. Noise, outliers, and mismatched low elevations were deleted and adjusted to optimize raster product generation during this supervised classification step. All developed features, such as buildings and structures, were omitted from the habitat analysis.

To produce a DSM, all points within the dense point cloud, ground and non-ground, were used to render the above- surface features, such as trees and vegetation. Also, a subset of points that represent the ground were interpolated to produce a continuous surface. For shadowed,

densely vegetated areas, resultant DTMs may have sparse or missing ground samples, and detected ground points may be unable to model the underlying surface with high accuracy [40].

nDSMs were derived by subtracting the DSM from the DTM. The local reference surface, or relative height, in the nDSM, is the surrounding ground surface represented by the corresponding DTM. In this study, only trees and low-statured vegetation are targeted; therefore, canopy height models (CHM) are synonymous with nDSM. The raw difference between the DSM and DTM was calculated, and no data values were masked. Areas external to the enclosure's fence were included in the overall photogrammetric processing but excluded in the analysis.

Evaluating the reliability of the nDSM generated from UAS imagery is challenging in the absence of reference data. Even more challenging is obtaining reference data on ground and canopy heights due to interference with signal strength from clustered and thick overhead canopies. To provide some insight and an assessment of quality, point cloud, DSM, and nDSM were visually inspected to detect any anomalies such as abrupt changes in elevation, inconsistencies in the elevation values, or artifacts caused by processing issues. In evaluating the discrepancies, we acknowledge the limitations of using only remotely sensed data for results and reporting.

Deriving Vegetation Structure Metrics

The following section of this research paper describes the methodology to: assign vegetation structure classes and gap analysis, identify individual trees and delineate canopy diameters using IWS, calculate vegetation indices for tree health diagnostics, and distinguish between tree species using spectral thresholding. The vegetation structure metrics derived and analyzed in this study are continuous value attribute image datasets representing vegetation canopy height and fractional canopy cover, referred to as "gaps." Photogrammetrically derived data used for the following analysis provides the basis of information on the 3D vertical and horizontal structure of Affenberg's vegetation, landscape heterogeneity, and fine-scale spatial representation of areas with varying degrees of cover.

Structure Classes and Gap Analysis

Canopy height data are summarized by mean height, top-of-canopy height, and height percentiles ranging from 5th to 95th percentiles in 5 m increments for grid units of analysis summarized below [16]. Structure classes were categorized based on height thresholds and growth patterns for species known to be present in the enclosure from literature review and visual

confirmation. Cells in the nDSM that reach approximately > 9 m were classified as tree canopy points, with ground cover (herbaceous plants and low vegetation) $0 - 0.5$ m, low shrubs (small shrubs and dense herbaceous vegetation) $0.5 - 1$ m, tall shrubs and young trees (small trees and mature shrubs) $1 - 3$ m, mid-height trees (sub-canopy layer, typically deciduous or younger trees) $3 - 10$ m, and tall trees (canopy and emergent layer, likely dominated by mature conifers) > 10 m (reference Figure 6 for visual representation of classes).

Percent canopy gap is the percentage of the ground that is not occluded by vegetation canopies per unit area [41]. A threshold of 9 m for the canopy heights is set to differentiate between the trees and non-tree vegetation and ground. Canopy gap is represented as a fraction from 0.00 (complete canopy cover) to 1.00 (complete gaps) for the $40,000 \text{ m}^2$ area as described below:

Equation 1: Canopy Gaps

$$CC = Av/Au$$

where:

Av = projected canopy gap area determined by the number of nDSM pixels classified as vegetation canopy within the $40,000 \text{ m}^2$ total area;

Au = total number of pixels within the $40,000 \text{ m}^2$ total area.

Individual Tree Identification and Delineation

Identifying individual trees can be challenging, depending on the size of a study site. As a baseline, we created a vector dataset of the trees in the enclosure, where we identified, and hand-digitized individuals above 9 m using visual interpretation of the T1 high-resolution orthomosaic. Due to the nature of this project, our study area was a small enough size making this process feasible and reasonably straightforward. This is the first dataset of trees for this enclosure and serves as a general inventory that did not exist prior to this project.

Utilizing ArcGIS Pro, we used the IWS technique to identify individual trees and to measure canopy diameters utilizing the T1 CHM. ITC3D performs well in coniferous forests, which suits this study, especially given the small spatial area being mapped. We first tested and implemented the IWS technique in the GIS mapping environment, and then after achieving results, the same geoprocessing workflow was designed in custom made visual code to automate and repeat image segmentation. This platform used, ModelBuilder is a visual programming language

for building workflows in ArcGIS; it is ideal for this project, where users are able to run the code with different temporal raster datasets to observe changes over time in the enclosure.

To conduct the IWS we first resampled the CHM from 5 cm to 0.5 m ground sampling distance (GSD) to be coarser resolution and lessen the noise in the watershed. We then detected the local maxima using a focal statistics tool. This isolates the highest pixel value on the treetop and eliminates multiple local maxima within a single crown area. This prevented a severe “over-segmentation” caused by multiple high peaks in a tree, such as multiple branches poking high in the sky [28]. When selecting cell units within a kernel range, it largely depends upon the resolution of the imagery. After some testing and resampling of the CHM, we chose a radius of 2 cells which is approximately 4 m GSD. We then created a Boolean raster to mark these treetops by matching them with the CHM values. We inverted the CHM so that the treetops became the lowest points, simulating water flow across a landscape. With the inverted CHM, we generated a flow direction raster to identify drainage basins, where treetops are “ponds,” and the branches and crowns became watershed areas. Based on the steepest downhill slope, we assigned the direction to be one of eight possible cardinal directions (N, NE, E, SE, S, SW, W, NW). We then applied a height threshold mask to refine the tree crown areas by selecting only regions above 9.3 m and then multiplied this Boolean mask with the watershed raster to isolate tree crown areas. This then created a final Boolean mask to retain only the tree crown values. Finally, we vectorized this last raster to generate points for each tree crown and added X and Y coordinates for spatial reference in further analysis. A detailed illustration of the step-by-step process in ArcGIS Pro is provided in Figure 4, and the final map of the IWS and hand-digitized individuals is seen in Figure 9.

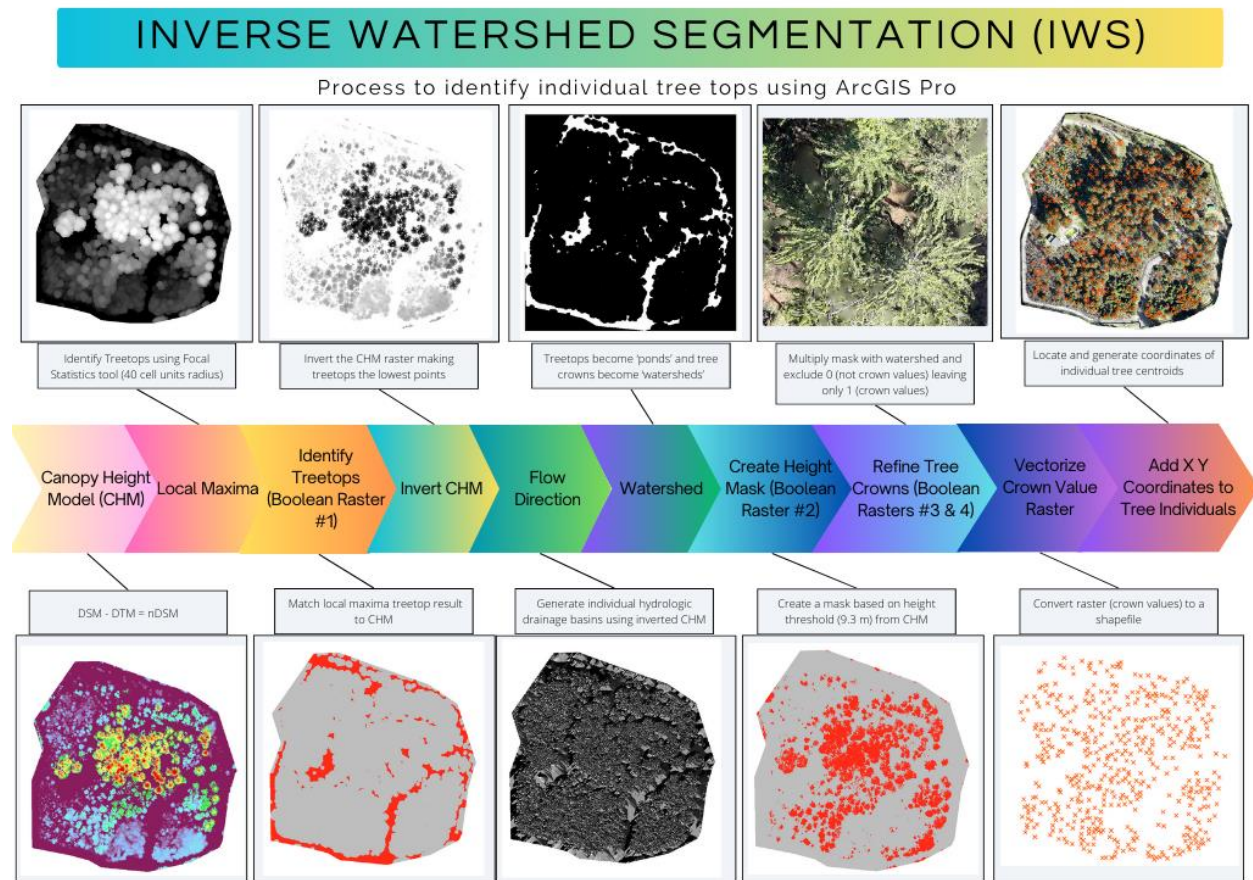


Figure 4: IWS Workflow

Similar to the iterative process of identifying individual treetops, we delineated the crown diameters using part of the IWS geoprocessing workflow. After inverting the CHM, we created a flow direction raster which we used to create basins. We then reclassified the original CHM into a binary raster based on a 9 m height threshold to differentiate between tree crowns and ground features. We multiplied the reclassified CHM with the basin raster, isolating areas within each basin that meet this height criteria. We then converted this tree crown raster into a polygon layer which turned each detected tree crown area into a vector object. From here, we generated centroids in each polygon, representing the approximate center of each tree crown. Then we extracted the vertices of each polygon to create points along the boundaries of each crown polygon. To determine the approximate diameter of each tree crown, we calculated the distance from each centroid to the nearest boundary point and amended this measurement to the attribute table. One of the major issues with this technique, however, was that the level of detail for individual canopies was too high, causing there to be way too many points. In order to reduce the number of vertices,

we simplified polygons using the cartographic refinement method by Douglas-Peucker, “Retain Critical Points.” This algorithm is a coarse simplification method that works by removing redundancies. Unfortunately, this method did not follow the canopy outlines completely and couldn’t preserve their character as closely but provided a rough approximation of each tree. Figure 5 displays canopy delineation examples using these GIS steps.

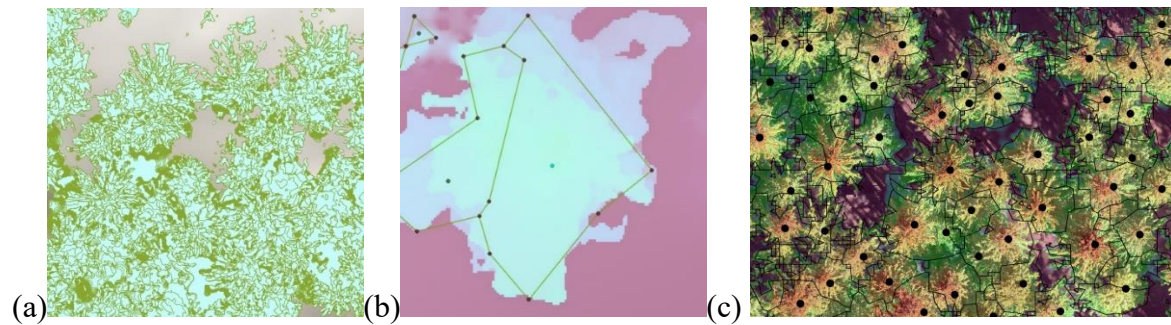


Figure 5: Canopy Measurement: a.) canopy polygons (teal) that are converted to lines (green); b.) simplified crown polygons (green lines) with centroids (teal dot); c.) CHM (rainbow) with polygon layer (black) and IWS tree points (black dots)

Tree Species and Health Assessment

A Normalized Difference Vegetation Index (NDVI) was calculated using the Micasense multispectral imagery to assess vegetation health and distinguish between evergreen and deciduous species. This SVI has historically been used to quantify and enhance vegetation health and stress, representing the spatial variations in the amount of photosynthetically illuminated plant material [42]. In calculating this index we used the band combinations as described in the formula below.

Equation 2: Normalized Difference Vegetation Index (NDVI)

$$NDVI = \frac{(NIR_{0.842} - R_{0.650})}{(NIR_{0.842} + R_{0.650})}$$

With:

NIR = Near-infrared band surface reflectance with Micasense center wavelengths (μm)

R = Red band surface reflectance with Micasense center wavelengths (μm).

To focus on only the trees within the enclosure, we generated a mask to exclude herbaceous species that could cause NDVI values to become oversaturated or misrepresentative of tree canopy health. Totally dependent upon the biogeographic conditions and seasonal contexts of our study area, the herbaceous plants had higher NDVI values due to their dense chlorophyll content, which

skewed the data when mixed with tree measurements. We found that this was especially so with the evergreen species which had much lower NDVI values than the surrounding grasses. In masking these species, we isolated the values specific to tree canopies, reducing potential noise and improving the reliability of our classification.

Using the IWS individual tree points layer, we created a 1- m radius circular buffer around each point. Zonal statistics were then calculated within these buffered areas, with the masked NDVI raster as the input value. This process produced a detailed map displaying individual NDVI values for each tree, as shown in Figure 13. The resulting visualization also highlighted the locations of dead or defoliated trees within the enclosure.

NDVI spectral thresholding was used to separate between evergreen and deciduous tree species. This technique can be effective but has its limitations due to lighting conditions during image acquisition, seasonality, and the specific ecosystem or phenomena of interest. The multispectral imagery used for this classification was taken in late summer when the lighting conditions can greatly change the reflectance values from the sun angles at that time of year. To classify tree species, we developed a custom cutoff tailored to the specific NDVI values in the T2b dataset, allowing us to create categories that reflect the two different tree species. This process involved iterative testing and validation using the high resolution orthomosaic to ensure accuracy. The NDVI thresholding in this analysis applied two main conditional statements: NDVI values that were greater than or equal to 0.45 were assigned a class value of 2 which represented deciduous trees, while values between 0.13 and 0.45 were categorized with a class value of 1 for evergreen trees. Pixels with NDVI values below 0.13 were excluded from the classification as they indicated dead or dying trees. This classification was performed using the Raster Calculator geoprocessing tool in ArcGIS Pro.

Results

Height model results can be visualized in Figure 6 for the T1 (April 4, 2024) leaf- off conditions and T2a (July 17, 2024) leaf- on conditions at Affenberg. CHMs overlay respective orthomosaics collected for each time period. Color coding highlights the highest points in red and lowest points in purple. Major differences can be observed in the central and southern areas of the enclosure, with more canopy coverage in T2. Note in this provided figure the illumination conditions for the T1 orthomosaic have heavier shadowing due to image capture conditions only

causing differences in the visual coloration and interpretation between rasters (refer to Appendix for larger details).

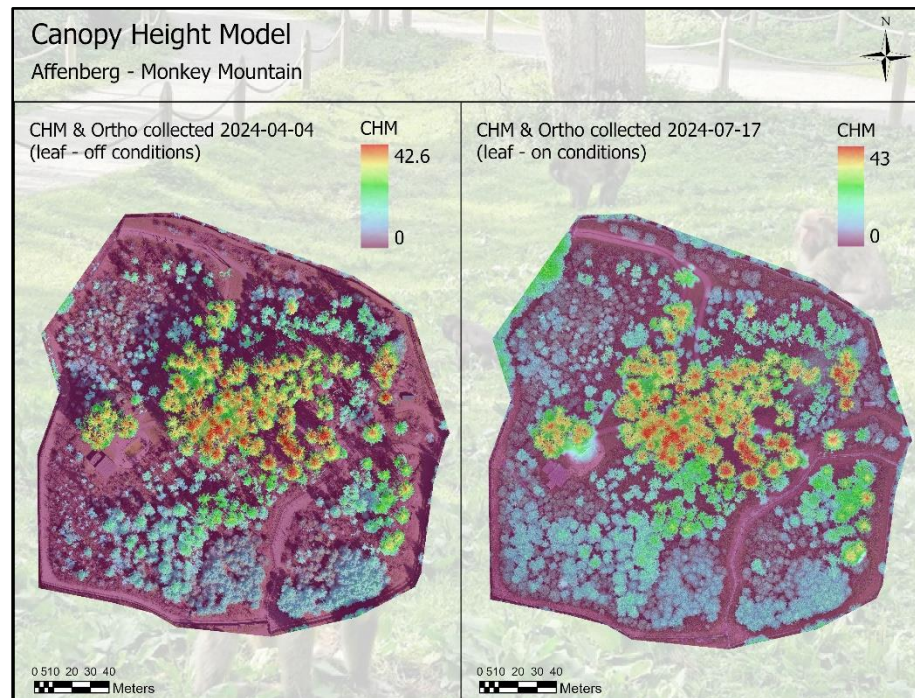


Figure 6: T1 & T2 Height Models (CHM) over respective orthomosaics (ortho); refer to Appendix for in larger detail maps

Behavioral studies using different scan methods are performed on the ground level to determine the optimal locations for after-dark protection and resting. Derived from the observational data on-site biologists have documented, the macaques predominantly inhabit the tallest trees in the center of the enclosure, closest to the feeding areas. Across the enclosure, the height ranges of 9 - 45 m can be inferred as potential sleeping spots, with Figure 7 providing a detailed illustration of the geographic distribution of these vegetation classes. The map highlights various height thresholds, from 9 - 15 meters up to 40 - 45 m, each represented by distinct colors. The darkest colors, blues, are the highest areas and the brightest colors, oranges, are the lowest areas of trees. This area is particularly significant for habitat suitability studies, as taller trees provide critical resources such as shelter during sleeping hours.

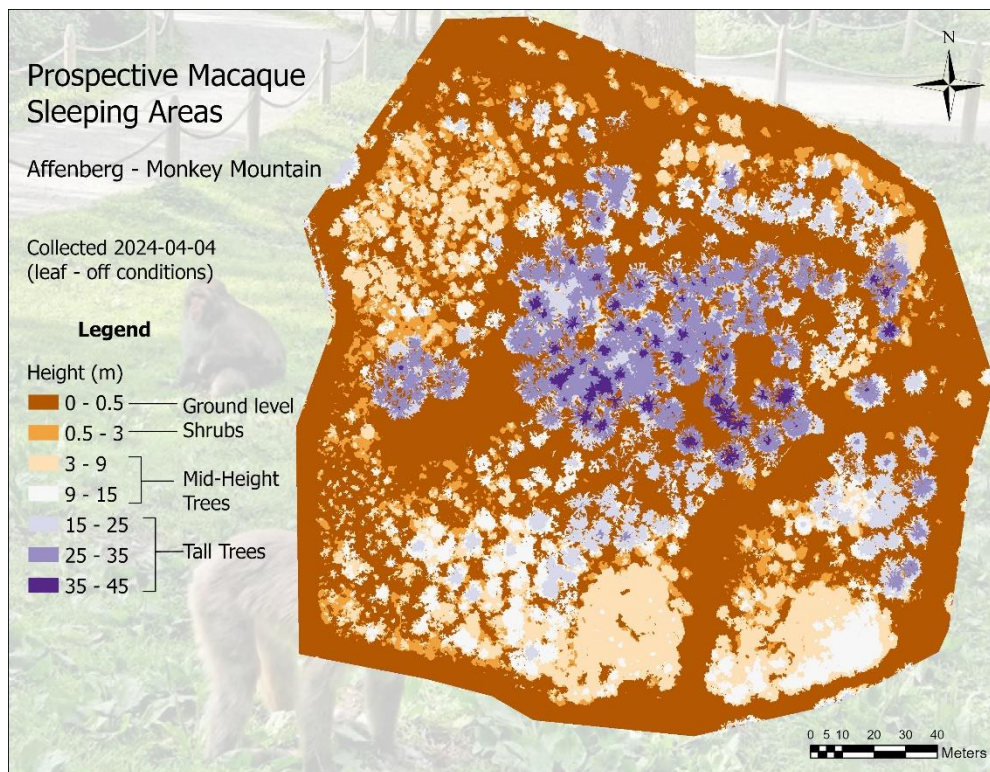


Figure 7: Canopy Height Model (CHM) map of potential sleeping locations

As seen in Figure 8, the vegetation structure in the enclosure shows a heterogeneous distribution of vegetation across the enclosure, highlighting varied structural complexity. The core section of the enclosure appears densely populated with tall shrubs and young, mid-height, and tall trees. This dense clustering indicates a high level of vertical habitat complexity, providing macaques with ample opportunities for foraging, movement, and shelter within a concentrated area. The spatial distribution of these trees, likely mature conifers, forms the top canopy and emergent layer. This promotes a higher likelihood of elevated pathways and secure vantage points, highlighting certain behavioral interactions. Towards the edges of the enclosure and central arteries, there are noticeable patches dominated by the gravel periphery boundary, ground cover, and low shrubs. These areas lack significant tree coverage, which limits their appeal for macaques' primary habitat zones. This gap area and low shrub zones also likely allow more sunlight to reach the ground, potentially influencing understory growth patterns. Overall, there is connectivity between low and high vegetation densities, a mixture of tall shrubs, young trees, and mid-height trees. The transitional areas create corridors for the macaques to use to navigate between parts of

the enclosure. This may reduce stress by allowing natural exploration and escape routes within the enclosure.

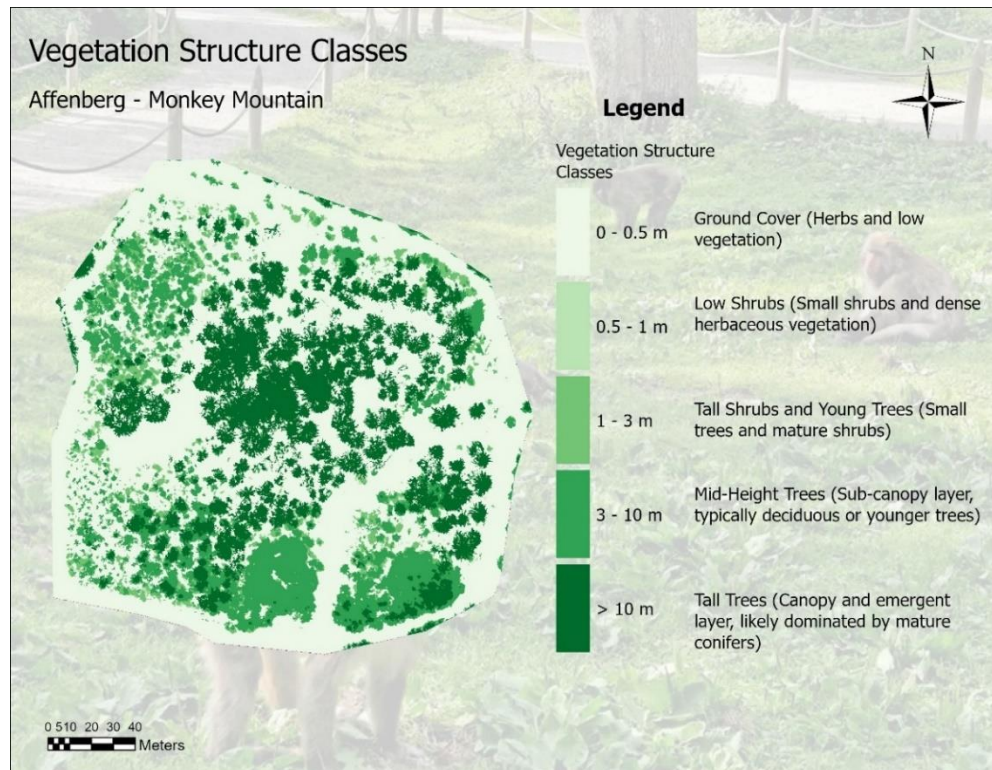


Figure 8: *Vegetation Structure Classification*

Figure 9 displays a map of the individual trees identified with blue crosses being manually digitized from visual interpretation of the leaf-off orthomosaic ($n = 463$), and red crosses being those identified using IWS ($n = 500$). The combined mapping of these provides a comprehensive view of the spatial distribution and coordinates of treetop locations. In comparing the two, the automated approach to locating treetops yielded 37 more individuals. This higher amount can be a product of the IWS algorithm's sensitivity to smaller or partially overlapping crowns, which may have been overlooked, clustered, or merged during manual digitization. This is especially the case with deciduous tree RGB shades and colors being closely related to those of shrubbery. There is also consistency and precision in using the IWS detection methods, ultimately avoiding any biases a manual approach might miss.

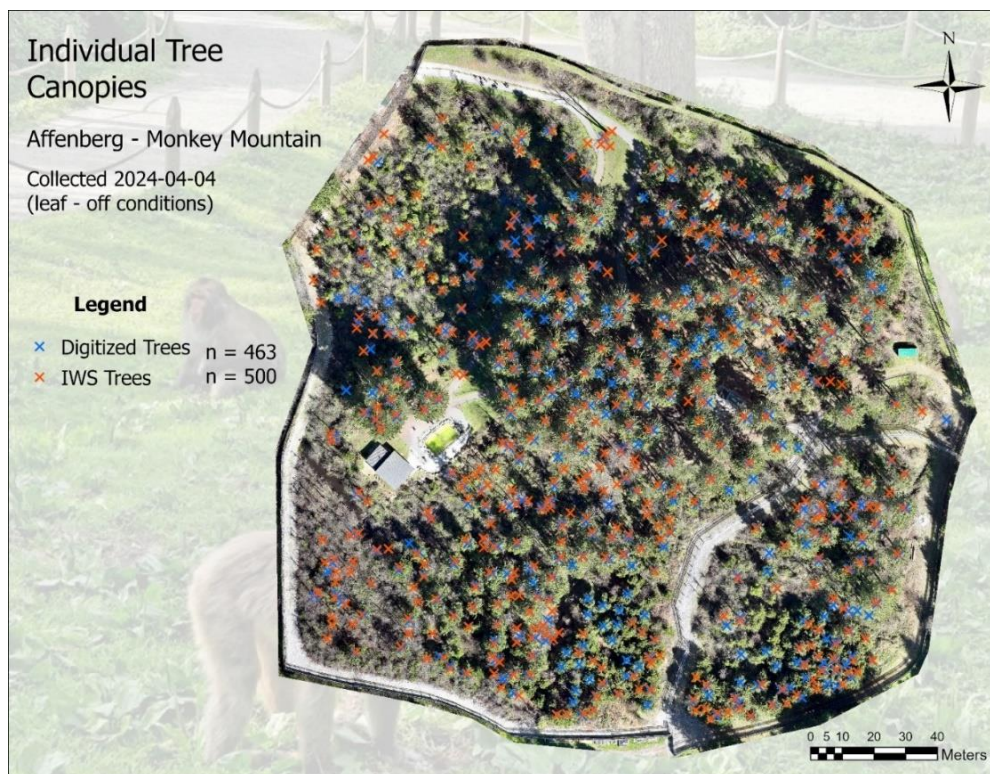


Figure 9: Individual Trees (Digitized vs IWS)

Figure 10 shows the distribution of evergreen and deciduous species overlaying the structure classes, providing a simplified representation of vegetation composition of forested areas. In total, there were 246 evergreen individuals, represented by an orange rounded-crown tree icon, and 202 deciduous individuals, represented by a purple triangle icon. Note that four individuals (indicated in Figure 13) were excluded from the total inventory due to being a standing dead or defoliated tree and more than likely not used for nocturnal cover by the macaques. Overall, this map indicates a pretty balanced distribution of the two, with the evergreen being evenly throughout the enclosure which presents a continuous canopy cover layer year round. This is particularly valuable for habitat stability in a region with a large diurnal range and provides shelter and visual protection all year round. The deciduous trees are interspersed among the evergreens contributing seasonal diversity to the habitat. This provides more food sources and shade during hot summer months.

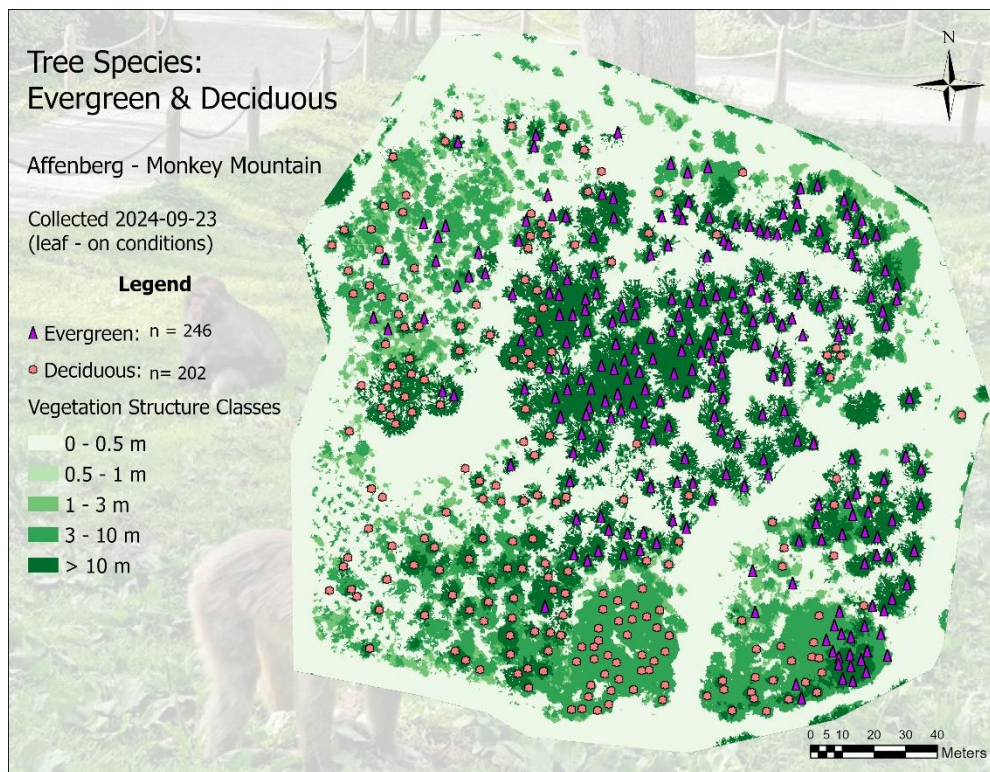


Figure 10: Tree species in structure classes: Evergreen & Deciduous

Determining open areas in the enclosure is key to understanding where in the macaque habitat certain behaviors are triggered. One such is the openness or “gaps” being where macaques choose to rest in the sun in a warm, sunny spot. The distribution of such potential places during leaf-on and leaf-off seasons can provide important information as to where they are spatially habituated and shifting seasonally. Maps of T1 (April 4, 2024, leaf-off conditions), T2 (July 17, 2024, leaf-on conditions), and year- round (January to December) canopy gaps are portrayed in Figure 11. Based on this analysis, there is almost a 20% change in canopy gap and openness in the enclosure between these time periods, offering more areas for macaques to be exposed to full sun or lie out for warmth. Most of this change is visible in the lower left quadrant, being mostly deciduous species, and the enclosure's upper right quadrant, a vegetative mixture. Year- round canopy gaps is, unsurprisingly, strongly symmetrical to the T2 periods, with only a 2% difference to leaf- off periods.

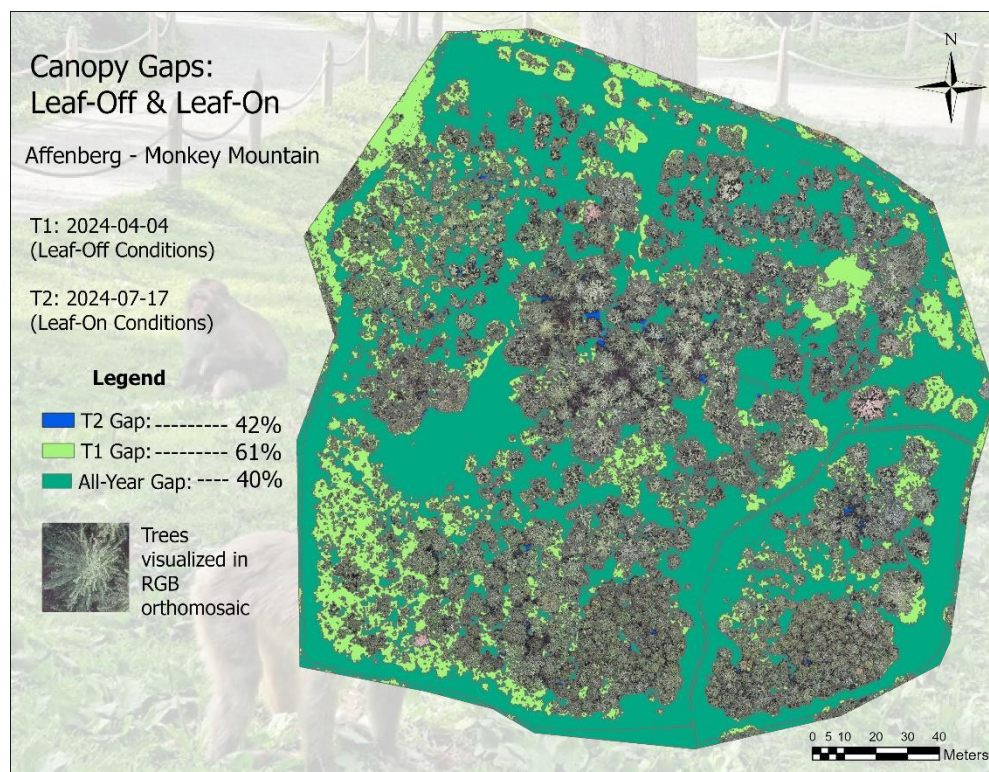


Figure 11: Canopy Gaps from T1 & T2 with the light green being the openness areas during leaf - off periods, the blue being leaf - on periods, and the darker green areas being year-round

The major differences seen for the T1 (April 4, 2024, leaf-off conditions) and T2 (July 17, 2024, leaf-on conditions) datasets can be visualized from Figure 12, highlighting seasonal changes in leaf density across the enclosure. In this map, red areas indicate the most significant increase in leaf coverage, likely reflecting deciduous trees that gained full foliage between spring and summer. This flush or increase in leaf density provides insights into the regions affected the most by seasonality. Areas without any color coding are regions where canopy coverage remained consistent across time frames, indicating no significant change. The very limited purple areas depict a decrease in leaf coverage which could result from natural shedding, dieback, stress from macaque overuse (or abuse), or other ecological factors. Another consideration for purple areas can be the results of interpolation artifacts introduced in the SfM reconstruction process. The SfM algorithm relies on overlapping photos to create the models, but where image overlap is limited, high shadowing, or missing data values are, interpolation is used to fill the gaps. This can create artificial reductions or inaccuracies in the CHM, which may influence the overall decrease in leaf coverage between datasets. These potential artifacts are seen in the core center of the enclosure

where the known tallest trees exist, confirming large shadowing and the suspected absence of data for raster products.

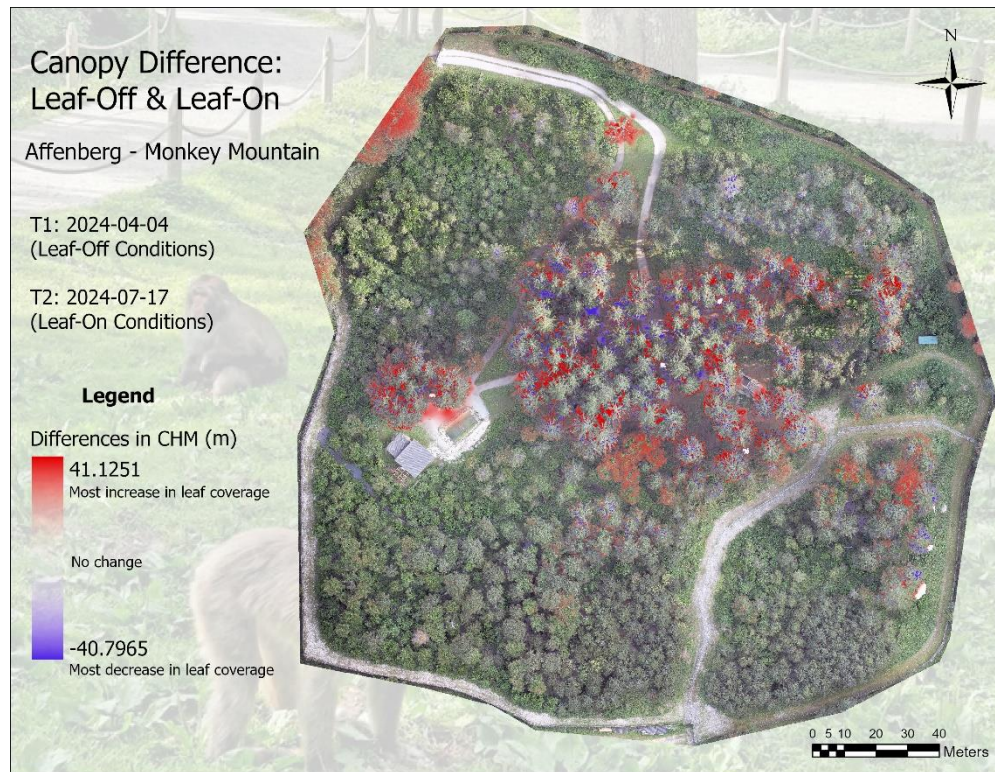


Figure 12: CHM changes between T1 & T2

Figure 13 enables an evaluation of individual tree health and assessment using NDVI. The SVI was calculated with leaf – on conditions with gap areas masked to only focus value ranges on trees. The chart below, Figure 14, depicts the frequency distribution of NDVI values, showing that most fall within the higher NDVI range. Additionally, specific trees identified as dead are symbolized with a red circle. However, areas of low and very low NDVI in red and yellow indicate areas of possible concern that may require targeted management efforts. When comparing Figure 10 results with Figure 13, it is noticeable that the deciduous trees show higher NDVI values than evergreen species. Deciduous trees tend to have higher reflectance activity due to leaf area, shape, and denser green foliage during the growing season.

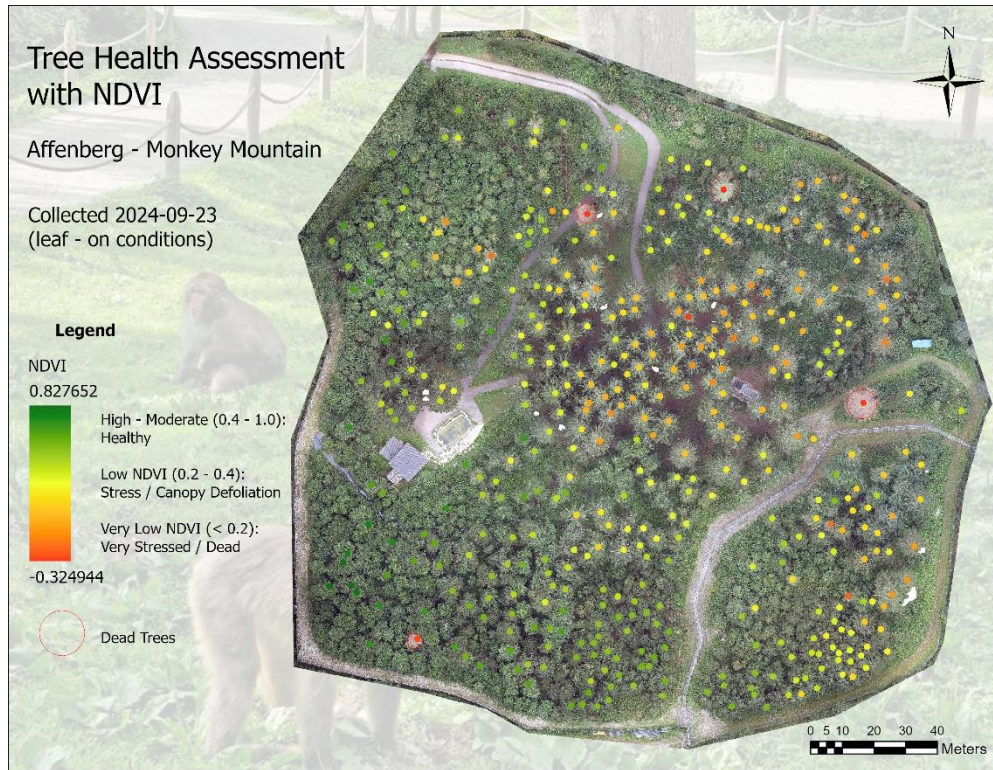


Figure 13: Tree Health Assessment using NDVI: Green areas represent high to moderate NDVI of 0.4 – 1.0, yellow areas with NDVI between 0.2 – 0.4, and red areas below 0.2.

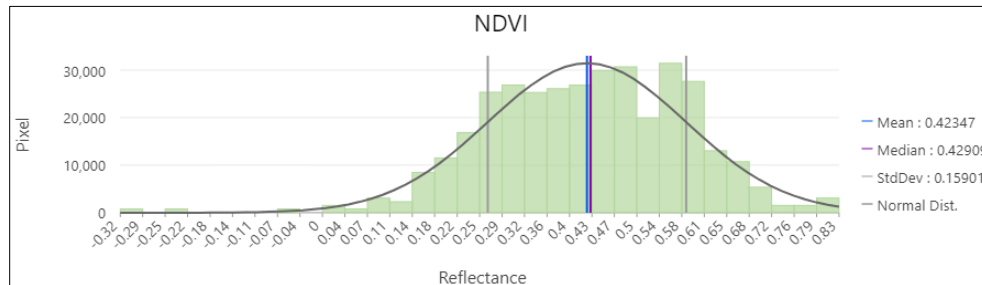


Figure 14: NDVI frequency distribution

Discussion

Implications for Wildlife Management

Ultimately, this study contributes to the knowledge base by leveraging advancements in technology, innovative methodologies, digital documentation, and newly available resources such as drones. These tools enable novel analyses and insights that were previously unavailable, particularly in the field of habitat monitoring for arboreal wildlife management. High-resolution digital images, videos, and sensor data collected through remote sensing tools like drones and GPS tracking devices provide detailed insights into animal behavior, movement patterns, and habitat usage with minimal disturbance to wildlife. Furthermore, this type of digital data collection can be

easily stored, shared, analyzed, and repeated. Facilitating collaboration across research teams and creating long-term datasets will support trends analysis and management decision making.

Canopy height models offer valuable insights into the vertical structure and complexity of vegetation. Macaques, like many arboreal and semi-arboreal species, often select habitats based on availability and arrangement of trees which serve as sources of food, shelter, and movement pathways. The zones with tall and complex canopies can pinpoint likely areas where macaques may prefer to forage, rest, or navigate. Complex canopies provide the vertical and horizontal diversity that macaques often seek for cover during nighttime colder temperatures. Such canopy height information can be linked to allometric equations, which estimate biomass and the potential availability of resources. These measurable features inform an empirical relationship between the allometric sizes of trees with locations for macaque behavior or preference. The larger, mature trees in the 30 – 45 m ranges make them likely focal points in macaque resting areas.

Challenges

Under high canopy cover, GNSS signals can be significantly weakened or obstructed, leading to low signal quality for point collection. Dense tree canopies can block or scatter the satellite signals, preventing the receiver from establishing a clear line of sight to the constellation. This obstruction increases the likelihood of signal reflections such as multipath errors. This ultimately prevented us from collecting precise ground survey measurements of individual trees and using this dataset for validation. In this small-scale study, broad vegetation structure zones or general areas provided sufficient information to understand and cross-reference the geolocations of macaque individuals; future studies can further explore and support their specific habitat preferences.

Some technical challenges that we encountered during this project were a geographic offset of T1 data and UAS image collection malfunction in T2 datasets. A geographic offset in the drone raster products refers to a spatial discrepancy between the actual geographic location of a feature on the ground and its represented location in the raster imagery. This can happen due to several factors from inaccuracies in the GPS data used during the drone flight, lack of ground control points (GCP), or slight misalignments introduced during the image stitching and processing. Our drone flights employed real-time kinematics (RTK) in the GPS of the platform, which helps refine the drone's positional data and reduce geographic offsets.

Also, in rare cases, real- world political or logistical conflicts can interfere with research objectives and consequently necessitate adaptation. In aircraft operations, careful monitoring of Notice to Air Missions (NOTAM) is imperative, as notices made about abnormal statuses of the Flight Information Region (FIR) made by the International Civil Aviation Organization (ICAO) can impact all personnel involved whether or not they are piloting a flight. This type of notification system alerts users of interference for all aircraft operations not excluding those using UAS. During the months between February 2024 to May 2024, several notifications were made in relation to the military invasion of Ukraine by the Russian Federation. This unique geo-political situation could have affected the aircraft sensors that collect RTK, causing a purposeful offset in GPS coordinates to prohibit or impede accurate geolocations (refer to the Appendix to view NOTAM referenced). To amend this issue, we had to correct the raster datasets using the GCPs we were able to collect in July. We performed the alignment in ArcGIS Pro using the Georeferencing toolset and manually positioning to match GCPs.

The second technical challenge we faced was during our July (T2a) image acquisition, wherein part of the multispectral images collected were missing part of the enclosure, inhibiting our ability to use that dataset for part of our study. The September (T2b) dataset used here was successful, however, this limited scope of multispectral analysis as processing and sharing resources was abbreviated to the conclusion of the Marshall Plan fellowship timeline.

Future Work

Building on the findings of this study, future work will aim to address the remaining gaps and explore the additional factors to enhance our understanding of Japanese macaque population dynamics and their habitat. Experimenting with different capturing positions and conditions with the UAS, such as viewing angles and monitoring wind conditions, could be worthwhile to obtain structure info. Oblique angles might highlight the understory vegetation obscured by dense canopy coverage undocumented using solely nadir- pointing perspectives [20]. Recent findings by Slade et al. (2024) have found wind speed to be a larger factor in SfM surveys and recommend an anemometer mounted at a standard height with a data logging function to record speed throughout the UAS survey [43].

Further work could focus on implementing more advanced Geographic Object-Based Image Analysis (GeoOBIA) models to enhance the detection and classification of tree types,

building upon the foundational OBIA approach used in this project. The combination of multispectral orthomosaics (spectral), dense point clouds (structural), and the IWS canopy crown points (spatial) information can be instrumental in this type of ecological and forestry study [29]. This integrated approach can provide a more in-depth biodiversity assessment, significantly reducing the need for manual interpretation and increasing the scalability of extensive datasets.

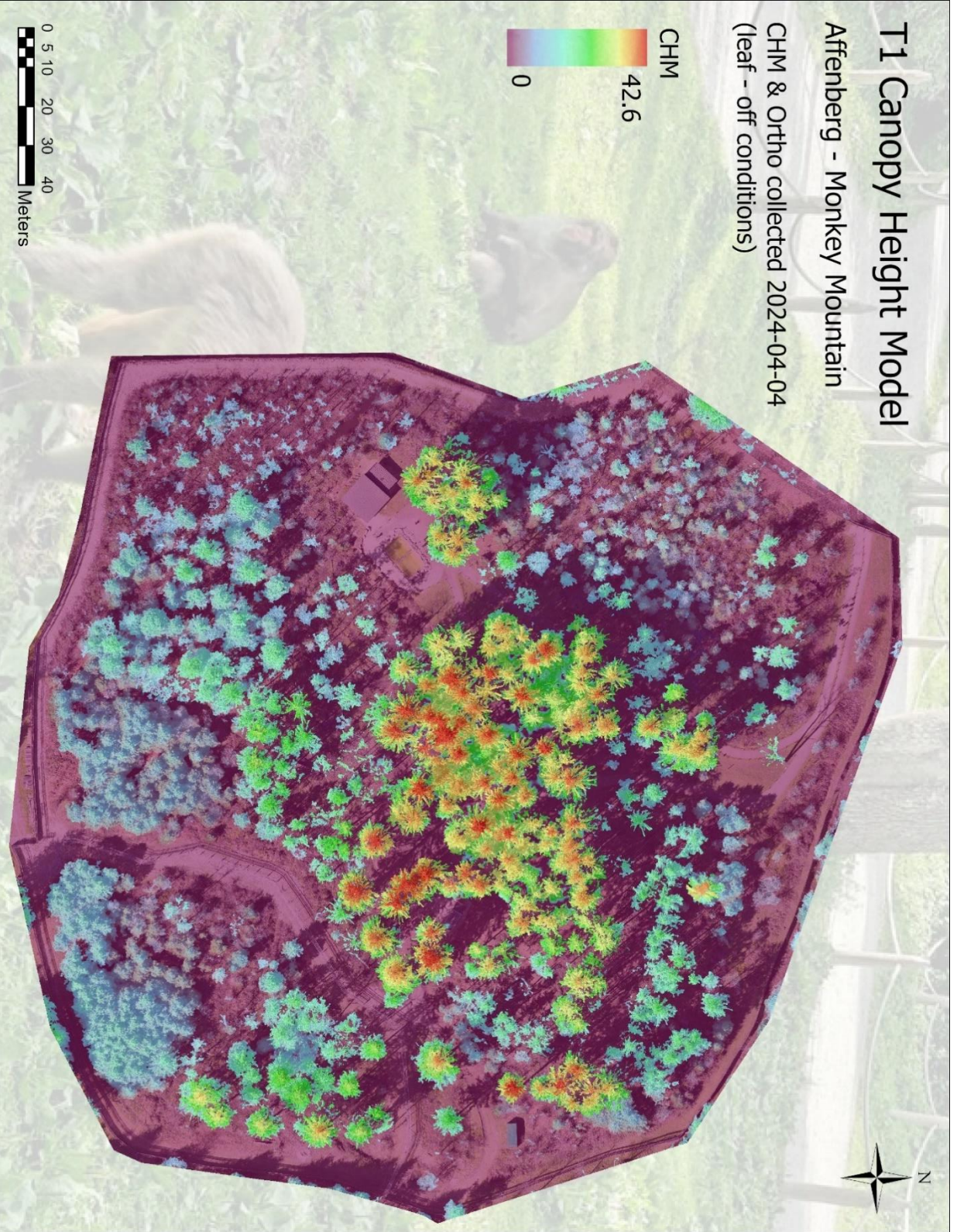
References

1. Sigmundson, R.; Stribos, M.S.; Hammer, R.; Herzele, J.; Pflüger, L.S.; Massen, J.J.M. Exploring the Cognitive Capacities of Japanese Macaques in a Cooperation Game. *Animals* **2021**, *11*, 1497, doi:10.3390/ani11061497.
2. Böhm, P.M.; Pflüger, L.S.; Pink, K.E.; Huffman, M.A.; Wallner, B. Intense Body Contact Increases Homosexual Pair Bond Stability in Female Japanese Macaques (*Macaca Fuscata*). *Arch. Sex. Behav.* **2024**, *53*, 1653–1665, doi:10.1007/s10508-023-02781-6.
3. Chen, H.L.; Lewison, R.L.; An, L.; Yang, S.; Shi, L.; Zhang, W. Understanding Direct and Indirect Effects of Payment for Ecosystem Services on Resource Use and Wildlife. *Anthropocene* **2020**, *31*, 100255, doi:10.1016/j.ancene.2020.100255.
4. Wood, E.M.; Pidgeon, A.M.; Radeloff, V.C.; Keuler, N.S. Image Texture as a Remotely Sensed Measure of Vegetation Structure. *Remote Sens. Environ.* **2012**, *121*, 516–526, doi:10.1016/j.rse.2012.01.003.
5. Nudds, T.D. Quantifying the Vegetative Structure of Wildlife Cover. *Wildl. Soc. Bull. 1973-2006* **1977**, *Vol. 5, No. 3*, 113–117.
6. Lechner, A.M.; Foody, G.M.; Boyd, D.S. Applications in Remote Sensing to Forest Ecology and Management. *One Earth* **2020**, *2*, 405–412, doi:10.1016/j.oneear.2020.05.001.
7. Dorren, L.K.A.; Maier, B.; Seijmonsbergen, A.C. Improved Landsat-Based Forest Mapping in Steep Mountainous Terrain Using Object-Based Classification. *For. Ecol. Manag.* **2003**, *183*, 31–46, doi:10.1016/S0378-1127(03)00113-0.
8. Iglhaut, J.; Cabo, C.; Puliti, S.; Piermattei, L.; O'Connor, J.; Rosette, J. Structure from Motion Photogrammetry in Forestry: A Review. *Curr. For. Rep.* **2019**, *5*, 155–168, doi:10.1007/s40725-019-00094-3.
9. Lawrence, B. Classifying Forest Structure of Red-Cockaded Woodpecker Habitat Using Structure from Motion Elevation Data Derived from sUAS Imagery. *Drones* **2022**, *6*, 26, doi:10.3390/drones6010026.
10. Tsai, Y.; Stow, D.; Chen, H.; Lewison, R.; An, L.; Shi, L. Mapping Vegetation and Land Use Types in Fanjingshan National Nature Reserve Using Google Earth Engine. *Remote Sens.* **2018**, *10*, 927, doi:10.3390/rs10060927.
11. Zisi, T.; Alexandridis, T.; Kaplanis, S.; Navrozidis, I.; Tamouridou, A.-A.; Lagopodi, A.; Moshou, D.; Polychronos, V. Incorporating Surface Elevation Information in UAV Multispectral Images for Mapping Weed Patches. *J. Imaging* **2018**, *4*, 132, doi:10.3390/jimaging4110132.
12. Camarretta, N. Monitoring Forest Structure to Guide Adaptive Management of Forest Restoration: A Review of Remote Sensing Approaches. *New For.* **2020**.
13. Dash, J.; Pearse, G.; Watt, M. UAV Multispectral Imagery Can Complement Satellite Data for Monitoring Forest Health. *Remote Sens.* **2018**, *10*, 1216, doi:10.3390/rs10081216.
14. Guo, X.; Wang, M.; Jia, M.; Wang, W. Estimating Mangrove Leaf Area Index Based on Red-Edge Vegetation Indices: A Comparison among UAV, WorldView-2 and Sentinel-2 Imagery. *Int. J. Appl. Earth Obs. Geoinformation* **2021**, *103*, 102493, doi:10.1016/j.jag.2021.102493.

15. Fraser, R.; Van Der Sluijs, J.; Hall, R. Calibrating Satellite-Based Indices of Burn Severity from UAV-Derived Metrics of a Burned Boreal Forest in NWT, Canada. *Remote Sens.* **2017**, *9*, 279, doi:10.3390/rs9030279.
16. Shin, P.; Sankey, T.; Moore, M.; Thode, A. Evaluating Unmanned Aerial Vehicle Images for Estimating Forest Canopy Fuels in a Ponderosa Pine Stand. *Remote Sens.* **2018**, *10*, 1266, doi:10.3390/rs10081266.
17. Lukas, S. Automated Recognition of Monkeys in Natural Habitats Using Convolutional Neural Networks (CNN).
18. Mirka, B.; Stow, D.A.; Paulus, G.; Loerch, A.C.; Coulter, L.L.; An, L.; Lewison, R.L.; Pflüger, L.S. Evaluation of Thermal Infrared Imaging from Uninhabited Aerial Vehicles for Arboreal Wildlife Surveillance. *Environ. Monit. Assess.* **2022**, *194*, 512, doi:10.1007/s10661-022-10152-2.
19. Cunliffe, A.M.; Brazier, R.E.; Anderson, K. Ultra-Fine Grain Landscape-Scale Quantification of Dryland Vegetation Structure with Drone-Acquired Structure-from-Motion Photogrammetry. *Remote Sens. Environ.* **2016**, *183*, 129–143, doi:10.1016/j.rse.2016.05.019.
20. Mathews, A.; Jensen, J. Visualizing and Quantifying Vineyard Canopy LAI Using an Unmanned Aerial Vehicle (UAV) Collected High Density Structure from Motion Point Cloud. *Remote Sens.* **2013**, *5*, 2164–2183, doi:10.3390/rs5052164.
21. Fawcett, D.; Azlan, B.; Hill, T.C.; Kho, L.K.; Bennie, J.; Anderson, K. Unmanned Aerial Vehicle (UAV) Derived Structure-from-Motion Photogrammetry Point Clouds for Oil Palm (*Elaeis Guineensis*) Canopy Segmentation and Height Estimation. *Int. J. Remote Sens.* **2019**, *40*, 7538–7560, doi:10.1080/01431161.2019.1591651.
22. Dandois, J.P.; Ellis, E.C. High Spatial Resolution Three-Dimensional Mapping of Vegetation Spectral Dynamics Using Computer Vision. *Remote Sens. Environ.* **2013**, *136*, 259–276, doi:10.1016/j.rse.2013.04.005.
23. Lisein, J.; Pierrot-Deseilligny, M.; Bonnet, S.; Lejeune, P. A Photogrammetric Workflow for the Creation of a Forest Canopy Height Model from Small Unmanned Aerial System Imagery. *Forests* **2013**, *4*, 922–944, doi:10.3390/f4040922.
24. Jayathunga, S.; Owari, T.; Tsuyuki, S. Digital Aerial Photogrammetry for Uneven-Aged Forest Management: Assessing the Potential to Reconstruct Canopy Structure and Estimate Living Biomass. *Remote Sens.* **2019**, *11*, 338, doi:10.3390/rs11030338.
25. Puliti, S.; Ørka, H.; Gobakken, T.; Næsset, E. Inventory of Small Forest Areas Using an Unmanned Aerial System. *Remote Sens.* **2015**, *7*, 9632–9654, doi:10.3390/rs70809632.
26. Tinkham, W.T.; Swayze, N.C. Influence of Agisoft Metashape Parameters on UAS Structure from Motion Individual Tree Detection from Canopy Height Models. *Forests* **2021**, *12*, 250, doi:10.3390/f12020250.
27. Panagiotidis, D.; Abdollahnejad, A.; Surový, P.; Chiteculo, V. Determining Tree Height and Crown Diameter from High-Resolution UAV Imagery. *Int. J. Remote Sens.* **2017**, *38*, 2392–2410, doi:10.1080/01431161.2016.1264028.

28. Miraki, M.; Sohrabi, H.; Fatehi, P.; Kneubuehler, M. Individual Tree Crown Delineation from High-Resolution UAV Images in Broadleaf Forest. *Ecol. Inform.* **2021**, *61*, 101207, doi:10.1016/j.ecoinf.2020.101207.
29. Prošek, J.; Šimová, P. UAV for Mapping Shrubland Vegetation: Does Fusion of Spectral and Vertical Information Derived from a Single Sensor Increase the Classification Accuracy? *Int. J. Appl. Earth Obs. Geoinformation* **2019**, *75*, 151–162, doi:10.1016/j.jag.2018.10.009.
30. Ustin, S.L.; Gamon, J.A. Remote Sensing of Plant Functional Types. *New Phytol.* **2010**, *186*, 795–816, doi:10.1111/j.1469-8137.2010.03284.x.
31. Taddeo, S.; Dronova, I.; Depsky, N. Spectral Vegetation Indices of Wetland Greenness: Responses to Vegetation Structure, Composition, and Spatial Distribution. *Remote Sens. Environ.* **2019**, *234*, 111467, doi:10.1016/j.rse.2019.111467.
32. Jennewein, J.S.; Eitel, J.U.H.; Joly, K.; Long, R.A.; Maguire, A.J.; Vierling, L.A.; Weygint, W. Estimating Integrated Measures of Forage Quality for Herbivores by Fusing Optical and Structural Remote Sensing Data. *Environ. Res. Lett.* **2021**, *16*, 075006, doi:10.1088/1748-9326/ac09af.
33. Iizuka, K.; Kato, T.; Silsigia, S.; Soufiningrum, A.Y.; Kozan, O. Estimating and Examining the Sensitivity of Different Vegetation Indices to Fractions of Vegetation Cover at Different Scaling Grids for Early Stage Acacia Plantation Forests Using a Fixed-Wing UAS. *Remote Sens.* **2019**, *11*, 1816, doi:10.3390/rs11151816.
34. Riihimäki, H.; Luoto, M.; Heiskanen, J. Estimating Fractional Cover of Tundra Vegetation at Multiple Scales Using Unmanned Aerial Systems and Optical Satellite Data. *Remote Sens. Environ.* **2019**, *224*, 119–132, doi:10.1016/j.rse.2019.01.030.
35. Fawcett, D.; Bennie, J.; Anderson, K. Monitoring Spring Phenology of Individual Tree Crowns Using Drone-Acquired NDVI Data. *Remote Sens. Ecol. Conserv. Vol. 7 Issue 2 P 227-244* **2020**.
36. Lisein, J.; Michez, A.; Claessens, H.; Lejeune, P. Discrimination of Deciduous Tree Species from Time Series of Unmanned Aerial System Imagery. *PLOS ONE* **2015**, *10*, e0141006, doi:10.1371/journal.pone.0141006.
37. Adamczyk, J.; Osberger, A. Red-Edge Vegetation Indices for Detecting and Assessing Disturbances in Norway Spruce Dominated Mountain Forests. *Int. J. Appl. Earth Obs. Geoinformation* **2015**, *37*, 90–99, doi:10.1016/j.jag.2014.10.013.
38. Pflüger, L.S.; Pink, K.E.; Wallner, B.; Radler, C.; Dorner, M.; Huffman, M.A. Twenty-Three-Year Demographic History of the Affenberg Japanese Macaques (*Macaca Fuscata*), a Translocated Semi-Free-Ranging Group in Southern Austria. *Primates* **2021**, *62*, 761–776, doi:10.1007/s10329-021-00928-4.
39. Tomašík, J.; Mokroš, M.; Saloň, Š.; Chudý, F.; Tunák, D. Accuracy of Photogrammetric UAV-Based Point Clouds under Conditions of Partially-Open Forest Canopy. *Forests* **2017**, *8*, 151, doi:10.3390/f8050151.
40. Iizuka, K.; Yonehara, T.; Itoh, M.; Kosugi, Y. Estimating Tree Height and Diameter at Breast Height (DBH) from Digital Surface Models and Orthophotos Obtained with an Unmanned Aerial System for a Japanese Cypress (*Chamaecyparis Obtusa*) Forest. *Remote Sens.* **2017**, *10*, 13, doi:10.3390/rs10010013.

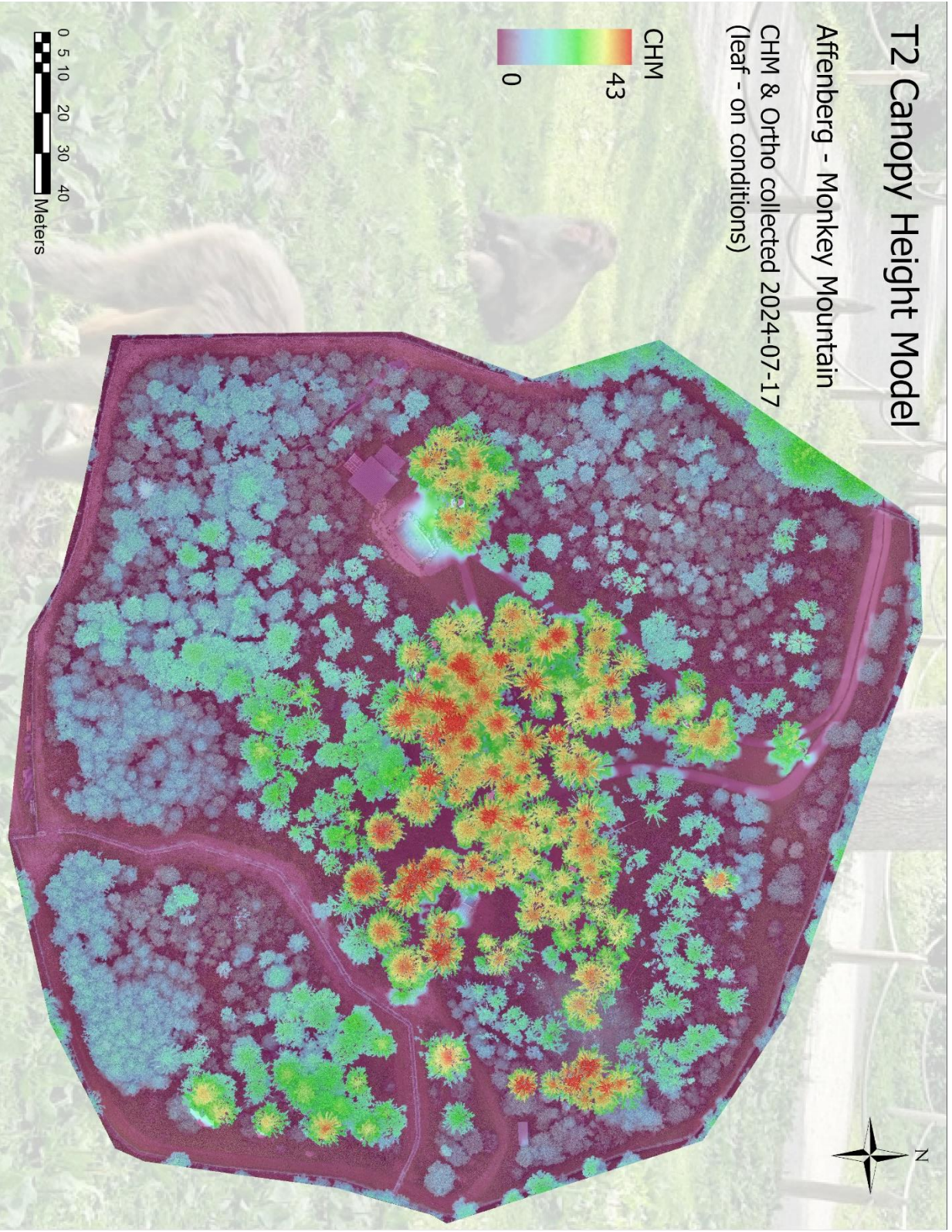
41. Crookston, N.L.; Stage, A.R. *Percent Canopy Cover and Stand Structure Statistics from the Forest Vegetation Simulator*; U.S. Department of Agriculture, Forest Service, Rocky Mountain Research Station: Ft. Collins, CO, 1999; p. RMRS-GTR-24;
42. Rouse, J.W.; Haas, R.H.; Deering, D.W.; Schell, J.A.; Harlan, J.C. Monitoring the Vernal Advancement and Retrogradation (Green Wave Effect) of Natural Vegetation, NASA/GSFC Type III Final Report, Greenbelt, MD. **1974**, 371p.
43. Slade, G.; Anderson, K.; Graham, H.A.; Cunliffe, A.M. Repeated Drone Photogrammetry Surveys Demonstrate That Reconstructed Canopy Heights Are Sensitive to Wind Speed but Relatively Insensitive to Illumination Conditions. *Int. J. Remote Sens.* **2024**, 1–18, doi:10.1080/01431161.2024.2377832.



T2 Canopy Height Model

Affenberg - Monkey Mountain

CHM & Ortho collected 2024-07-17
(leaf - on conditions)





DFS Deutsche Flugsicherung

Bundesrepublik
Deutschland

PIB

AIS-Portal
PilotService

ROUTE TYPE

ID EDDZ2405160586

Prepared on 16 May 2024 06:10 UTC

DEEWE

Flightrules	VFR
Departure aerodrome	EDMO/OBERPFAFFENHOFEN
Destination aerodrome	EDDB/BERLIN BRANDENBURG
Alternate aerodromes	EDDH/HAMBURG
Crossed FIRs	EDMM EDWW
Validity	From 16 May 2024 06:10 UTC until 17 May 2024 06:10 UTC
No NOTAM about	OBSTACLE, OBSTACLE LIGHTS
Note	<p>*NOTAM marked with only one red asterisk are shown in reduced view on users request.</p> <p>**NOTAM which are valid for several FIRs are only fully displayed at the first appearance in the briefing. For other FIRs they appear in reduced form.</p>

6

EDWW EDGG EDMM FLIGHT INFORMATION REGION (FIR)**B0266/24***From 15 Apr 2024 08:44 until 16 May 2024 23:59*

SECURITY - HAZARDOUS SITUATION IN SOMALIA
 CIVIL GERMAN AIR OPERATORS ARE RECOMMENDED NOT TO ENTER FIR MOGADISHU
 (HCSM) BELOW FL260. POTENTIAL RISK FROM ANTI-AVIATION WEAPONRY,
 MILITARY OPERATIONS AND ARMED CONFLICTS.
 EXCLUDED FROM THIS RECOMMENDATION IS THE AREA EAST OF LONGITUDE
 E0540000.
 THIS NOTAM OVERRULES THE RECOMMENDATION PROVIDED IN AIC 03/24.

EDWW EDGG EDMM FLIGHT INFORMATION REGION (FIR)**B0263/24***From 12 Apr 2024 13:22 until 17 May 2024 23:59*

HAZARDOUS SITUATION IN IRAN
 CIVIL GERMAN AIR OPERATORS ARE RECOMMENDED NOT TO ENTER FIR TEHRAN
 (OIIX). POTENTIAL RISK FROM ESCALATING CONFLICT AND ANTI-AVIATION
 WEAPONRY. THIS NOTAM OVERRULES THE RECOMMENDATION PROVIDED IN AIC
 03/24.

EDGG EDMM EDWW FLIGHT INFORMATION REGION (FIR)**B0237/24***From 03 Apr 2024 14:15 until 02 Jul 2024 23:59 EST*

MILITARY INVASION OF UKRAINE BY RUSSIAN FEDERATION.
 REROUTINGS, EXTENDED ROUTE PORTIONS BELOW FL245 AND DELAY MAY BE
 EXPECTED WITHIN LOWER AND UPPER GERMAN AIRSPACE
 DUE TO AIRSPACE RESTRICTIONS FOR THE EXECUTION OF MILITARY MISSIONS.
 IT IS RECOMMENDED TO CONSIDER THE USE OF EXTRA-FUEL.

EDGG EDMM FLIGHT INFORMATION REGION (FIR)**B0141/24***From 07 Mar 2024 12:04 until 06 Jun 2024 23:59 EST*

PUBLICATION OF CTA/UTA IN DELEGATED AIRSPACE OVER AUSTRIAN
 TERRITORY:
 IN GERMAN AIP CTA/UTA DATA ARE PUBLISHED IN ENR 2.1. EVEN SO CTA/UTA
 ARE DESCRIBED CONSISTING OF THE FOLLOWING SECTORS, MUENCHEN CTA AND
 KARLSRUHE UTA END AT THE GERMAN-AUSTRIAN BORDER AND ARE NOT VALID
 OVERHEAD WIEN FIR.
 PUBLISHED BOUNDARIES OF ATC SECTORS EDUUALP 14-44, EDUUCHI 14-44,
 EDMMZUG, EDMMTEG, EDMMTRU AND EDMMSTA ARE NOT AFFECTED.
 (AIP GERMANY PAGES ENR 2.1-84FF REFERS).

EDWW EDGG EDMM FLIGHT INFORMATION REGION (FIR)**B0121/24***From 28 Feb 2024 08:16 until 28 May 2024 08:00 EST*

MILITARY INVASION OF UKRAINE BY RUSSIAN FEDERATION:
 NOTE 1: ALL AIRCRAFT OWNED, CHARTERED OR OPERATED BY CITIZENS OF THE RUSSIAN FEDERATION OR OTHERWISE CONTROLLED BY NATURAL OR LEGAL PERSONS OR ENTITY FROM THE RUSSIAN FEDERATION AND OPERATORS HOLDING AIR OPERATOR CERTIFICATE (AOC) ISSUED BY THE RUSSIAN FEDERATION AUTHORITIES ARE PROHIBITED TO ENTER, EXIT OR OVERFLY GERMAN AIRSPACE EXCEPT HUMANITARIAN FLIGHTS WITH THE PERMISSION OF THE GERMAN MINISTRY FOR DIGITAL AND TRANSPORT AND IN CASE OF EMERGENCY LANDING OR EMERGENCY OVERFLIGHT. REQUESTS FOR HUMANITARIAN FLIGHTS SHALL BE SENT TO HUM-FLIGHTS(AT)DFS.DE WITH DATE, EOBT, ADEP AND ADES.
 NOTE 2: AIRCRAFT OPERATORS OF NON-SCHEDULED FLIGHTS BETWEEN RUSSIA AND GERMANY, OPERATED DIRECTLY OR VIA A THIRD COUNTRY, MUST NOTIFY ALL RELEVANT INFORMATION CONCERNING THE FLIGHT PRIOR TO THEIR OPERATION AND AT LEAST 48 HOURS IN ADVANCE TO THE FEDERAL MINISTRY OF DIGITAL AND TRANSPORT. REQUIRED DOCUMENTS: FLIGHT PLAN, GENDEC, PAX LIST, IN CASE OF CARGO FREIGHT LIST AND AIR WAYBILL, COPY OF IDENTIFICATION DOCUMENTS AND VISAS OF ALL PASSENGERS AND CREW ON BOARD, CHARTER CONTRACT FOR THE AIRCRAFT, COST BEARER OF THE FLIGHT (IF A LEGAL ENTITY: DETAILS OF THE NATURAL PERSON ULTIMATELY RESPONSIBLE FOR FINANCIAL TRANSACTION IN THE LEGAL ENTITY), COPY OF RUSSIAN AUTHORISATION FOR THE USE OF RUSSIAN AIRSPACE. IN CASE OF HOSP OR MEDIVAC FLIGHTS CONFIRMATION OF RECEIVING HOSPITAL.
 NOTE 3: CONTACT FOR NOTIFICATION AND DOCUMENTS
 GERMANY-AVIATION-SANCTIONS(AT)BMDV.BUND.DE.

EDMM EDPR AIR/GROUND FACILITY OPERATING FREQUENCIES CHANGED**C1213/24***From 11 Apr 2024 12:15 until PERM*

AFIS AIRBUS INFORMATION 267.800MHZ CHANGED TO 241.000MHZ.
 REF AIP AD 3 EDPR 1-4 DATED 16 JUN 2022 AND AIP VFR AD 3 EDPR 1 DATED 04 JUN 2020.

EDWW EDMM UNMANNED AIRCRAFT FLYING WILL TAKE PLACE**D1270/24***From 15 May 2024 14:26 until 30 Jun 2024 21:00*

DAILY 0130-2100

UAS OPERATION 14.5NM RADIUS CENTERED ON 5150N 01427E COTTBUS (35NM ESE KLASDORF DVOR/DME KLF). OPERATING BVLOS.

GND up to 394FT AGL

EDWW EDMM UNMANNED AIRCRAFT FLYING WILL TAKE PLACE**D1269/24***From 15 May 2024 14:24 until 30 Jun 2024 21:00*

DAILY 0130-2100

UAS OPERATION 14NM RADIUS CENTERED ON PSN 5138N 01425E (39.4NM SE KLASDORF DVOR/DME KLF). OPERATING BVLOS.

GND up to 394FT AGL

EDMM EDDM ASCENT OF FREE BALLOON WILL TAKE PLACE**D1255/24***From 16 May 2024 12:00 until 16 May 2024 13:00*

ASCENT OF 16 TOY BALLOONS PSN 481919N 0113605E, ECHING (12.1NM NW OTTERSBERG DVOR/DME OTT).

GND up to FL100